Journal of Power Sources 258 (2014) 54–60

Contents lists available at ScienceDirect

Journal of Power Sources

journal homepage: www.elsevier.com/locate/jpowsour

Short communication

A new class of amorphous cathode active material $Li_xM_yPO_z$ (M = Ni, Cu, Co, Mn, Au, Ag, Pd)

Yuichi Sabi [a,*], Susumu Sato [b], Saori Hayashi [b], Tatsuya Furuya [b], Susumu Kusanagi [b]

[a] Activation Office, R&D Platform, Sony Corporation, Atsugi-shi, Kanagawa 243-0014, Japan
[b] Advanced Materials Laboratories, R&D Platform, Sony Corporation, Atsugi-shi, Kanagawa 243-0014, Japan

HIGHLIGHTS

- A new class of amorphous cathode active material is reported for the first time in detail.
- The composition margin is very wide, which is essential property from industrial point of view.
- The maximum capacity was 330 mAh g^{-1} for LiNiPO.
- High speed charging and discharging was performed upto 30 C.

ARTICLE INFO

Article history:
Received 5 December 2013
Received in revised form
3 February 2014
Accepted 6 February 2014
Available online 15 February 2014

Keywords:
Amorphous cathode active material
High-capacity cathode
Positive-electrode material
Sputter deposition
Thin film
Lithium-ion battery

ABSTRACT

A new class of amorphous cathode active material $Li_xM_yPO_z$ (LiMPO) is proposed. The materials are sputter deposited to thin film form by Li_3PO_4 together with metal or metal oxide targets. Among several materials tested as thin-film battery, working material found are M = Ni, Cu, Co, Mn, Au, Ag, Pd. The property is intensively studied for $Li_xCu_yPO_z$ (LiCuPO) and $Li_xNi_yPO_z$ (LiNiPO). Those materials shows wide composition margin such as composition y between 1 and 3, and high capacity for LiNiPO with maximum value of 330 mAh g^{-1}. The capability to charge and discharge at high rate is shown up to 30 C. This preliminary report reveals its high potentiality for further optimization.

1. Introduction

Lithium-ion batteries are commercialized worldwide and the market is increasing for various uses from small portable electronic devices to large scale system of electric vehicles. The key characteristic of the Li-ion battery is its high energy density. There is still strong demand for even higher energy density, and the quest for new active materials is subjected to intensive research.

The most common cathode active material (positive-electrode material) commercialized in the Li-ion battery industry is $LiCoO_2$ with distorted rock-salt crystal structure [1]. Other common cathode active materials are $LiMn_2O_4$ with spinel structure [2] or $LiFePO_4$ with olivine structure [3,4], both developed and commercialized with the merit of lower cost and safeness. For higher energy density, several other materials are proposed. However, most of the reports are based on metal-oxide crystal materials [5,6] or sulfides [7], and very limited number of amorphous oxide cathode active materials have been reported [8–10].

Among the amorphous cathode active material reported to date, vanadium oxide shows relatively fair characteristics such as high stability and high cycle durability. On the other hand, the potential of the material against Li metal is lower than 3 V and the voltage linearly decreases according to Li concentration in the material [10], and that limits the practical versatility.

Other well-known amorphous Li conducting material is the electrolyte LiPON [8]. Such amorphous materials have not yet been intensively studied for its additive materials and its composition possibilities, one reason by the difficulty of analyzing its mechanism because of its amorphous complexity. We report here a new

* Corresponding author. 7-5-15 Kinuta, Setagaya-ku, Tokyo 157-0073, Japan. Tel.: +81 70 5473 3198.
E-mail address: Yuichi.Sabi@gmail.com (Y. Sabi).

http://dx.doi.org/10.1016/j.jpowsour.2014.02.021
0378-7753/

class of amorphous cathode active material based on Li_3PO_4 composed with various metal materials, toward the composition far off from known crystalline materials.

Amorphous materials are usually prepared using rapid-quenching method such as melt-spinning or sputter deposition. For the oxide amorphous material, vacuum process is advantageous in respect to its property reproducibility and stability. The amorphous cathode active materials in this study are prepared by sputtering process, and measured by the form of thin-film battery. This system is advantageous in revealing the basic material property since the thickness and the surface boundary are well controlled under vacuum process [11–17].

The sputtered amorphous materials have the advantage that there is no need to post-anneal. That reduces the production process step, and enables usage of thin organic base films as substrate.

2. Experimental

The thin film batteries, including the new amorphous cathode active materials, were sputter deposited using Ulvac SMO-01 or Canon Anelva C-3103 sputtering machine [18,19]. Obtained characteristics were almost identical between these apparatuses.

The cathode active material was co-sputtered using Li_3PO_4 target together with a metal, metal oxide, or lithium metal oxide target (e.g. Ni, NiO, or $LiNiO_2$). The composition of metal M and oxygen are varied by sputtering conditions and the obtained $Li_xM_yPO_z$ (LiMPO) are investigated in several compositions. No other additives are added in those sputtering target materials or in the film.

The metal materials investigated were Mg, Al, Si, Ti, V, Cr, Mn, Fe, Co, Ni, Cu, Zn, Ga, Zr, Pd, Ag, Hf, W, Au, and Gd. Among those the most intensively studied materials were LiCuPO and LiNiPO.

The composition y of the metal against phosphor (M/P) was controlled mainly by sputtering power ratio between Li_3PO_4 and the metal containing target. Sputtering gas was Ar or Ar + O_2, at typical total pressure of 0.2 Pa. Oxygen content of the sputter gas was controlled depending on the desired oxygen content. For example, sputtering using a metal target at high power may result in lack of oxygen with Ar gas. In such case, Ar with O_2 gas of 20% partial pressure was used to stabilize the oxygen content in the sputtered film.

To measure the property of the sputtered cathode active material, a thin film battery was formed. All thin films were sputter deposited on polycarbonate substrate of 1.1 mm thickness. Cathode current collector (Ti), cathode active material, electrolyte (LiPON), and anode current collector (Cu/Ti) were consecutively deposited as depicted schematically in Fig. 1. Metal masks (stainless steel, 0.3 mm thick) were placed on the substrate to form a desired design of each layer. The shape of cathode active material was square with 8 mm × 8 mm size, with all area covered with current collectors and electrolytes. Anode current collector was separated to two layers to improve the cycle durability [15]. Typical sputtering conditions of each layer are described in other publications [18,19]. The anode active material in this system is the plated Li layer appears after charging. The anode Li plating behavior was observed by *in-situ* TEM in our previous study [17].

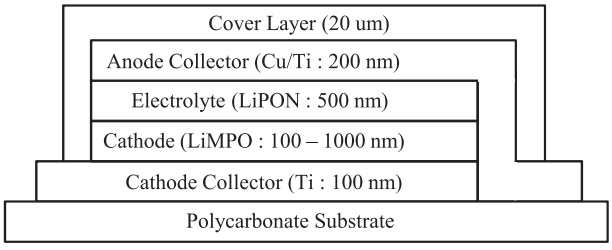

Fig. 1. Schematic diagram of a thin film battery cell.

After the thin film battery deposition the cell is covered with UV curable resin as protective layer. The role of this material is not only for scratch and moisture protection [16] but to suppress the anode collector surface from uncontrolled deformation by Li plating during charging process [13,14].

The composition of obtained cathode active material is measured with X-ray photoelectron spectroscopy (XPS), Rutherford backscattering spectrometry (RBS), and inductively coupled plasma-atomic emission spectroscopy (ICP-AES). Since the non-stoichiometric amorphous oxide material is relatively unstable regarding the oxygen bonding, the procedure of surface etching during XPS measurement may lead to offsetting of content. We have tested the content mainly by XPS [18,19], however, combining the RBS and ICP-AES method the obtained composition were presumed more accurate considering the valence balance inside the film. All XPS data in this report are thus calibrated to the value of RBS and ICP-AES method for consistency.

Charging/discharging and cyclic voltammetry curves (CV) were measured using TOSCAT (Toyo-system) and digital sourcemeter 2400 (Keithley). Electrochemical impedance spectroscopy (EIS) was measured with Solartron SI-1287 and SI-1260.

3. Result and discussion

3.1. a-LiCuPO

The sputtering target materials used in this experiment were Li_3PO_4 and Cu metal. The composition of the film was controlled by changing the sputtering power between Li_3PO_4 and Cu. The composition ratio of Cu and P is dependent linearly on power. Then the Li and O composition depend on the Cu/P atomic ratio and other sputtering conditions such as oxygen partial pressure of sputtering gas, and settle to neutral valence composition.

Film densities for different Cu/P compositions were measured using X-ray Reflectometer (XRR). As shown in Fig. 2, the film densities showed relatively moderate dependency against Cu/P content. Note that the fitting accuracy of the XRR measurement is below 1%, however, the existence of few nm surface oxidation layer and the surface roughness reduces the measurement accuracy down to about 5%. The film density measurement error corresponds to the accuracy of the cathode active material's maximum capacity shown in the following results. To clarify the uniformity

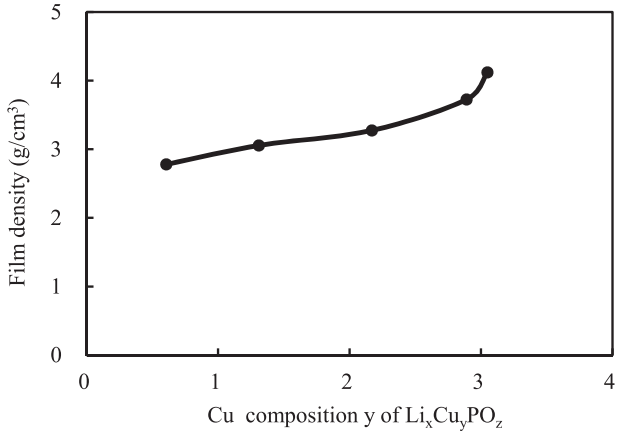

Fig. 2. Film density of LiCuPO film for different Cu/P compositions.

and amorphousness of the cathode active material, high resolution TEM and electron beam diffraction image was obtained for a material with composition of $Li_{2.6}Cu_{2.1}PO_{6.3}$ (Fig. 3). There was no appearance of any crystal phases found in the TEM image, and no diffraction satellite was observed. The film was proved to be a complete amorphous phase.

Typical charge and discharge curve is shown in Fig. 4 for a cell with 365 nm thick $Li_{2.6}Cu_{2.1}PO_{6.3}$. The horizontal axis was normalized by a film density interpolated from Fig. 2, and the film thickness measured separately for the sample prepared for each purpose. The maximum capacity of this cathode active material is estimated as 120 mAh g^{-1}, with output voltage shown above 3 V versus Li metal. Charge and discharge current were both 50 μA for 10 mm × 10 mm size area sample, thus corresponding to 3.4 C speed. Cut-off voltage for charging was set as 5.0 V. The operation voltage was determined considering a stability window of LiPON (0–5.5 V) [20]. At 120 mAh g^{-1} capacity, the Li content inside LiCuPO corresponds to Li/P = 1.3. A steep voltage increase near 120 mAh g^{-1} during charging implies that this material has high impedance nearby $Li_1Cu_{2.1}PO_{6.3}$ composition.

At this charging and discharging condition, cycle durability was measured (Fig. 5). The capacity decay became relatively stable after 20 cycles. There was no degradation found for the surface morphology of anode collector metal and UV resin cover, or any decay of LiPON layer as observed by TEM. The decay in capacity is considered mainly due to LiCuPO layer, since some additive materials effectively improved the cycle durability [19].

By changing the sputtering power of Cu target, a capacity dependence on composition of Cu against P is observed as Fig. 6. The working composition is relatively wide compared to crystal phase materials, since the capacity was stable between Cu/P = 1.2 to 2.5. That will be advantageous for mass production point of view. Below Cu/P = 1, the capacity decreases steeply due to lower electronic conductivity, as the composition become closer to amorphous Li_3PO_4 electrolyte.

Impedance spectrum was measured at discharged state as shown in Fig. 7. By comparing the spectrum between samples with different LiPON thicknesses, the spectrum circle at higher frequency, centered 36 kHz, is identified as LiPON origin. The conductivity was calculated as 3×10^{-7} S cm^{-1}, which is one digit lower than well-known value [8] presumably due to insufficient optimization of sputtering conditions. The second circle with center frequency of 400 Hz was thus considered as LiCuPO cathode active layer. The conductivity is estimated as 4.4×10^{-8} S cm^{-1}. For the cathode active layer with sub-micron thickness, the conductivity of such order will be negligibly small at 3.4 C charging or discharging. Since the impedance drop observed in Fig. 4 is in the order of 1 V, Li content gradation inside the film may have caused the Li vacant layer and increased the total resistance.

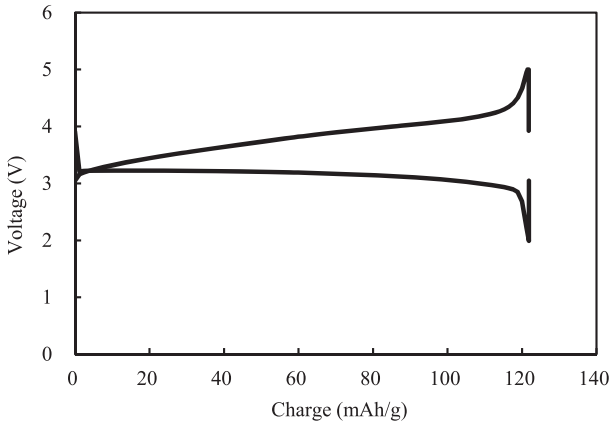

Fig. 4. Typical charge and discharge curves of a cell with $Li_{2.6}Cu_{2.1}PO_{6.3}$ cathode active material.

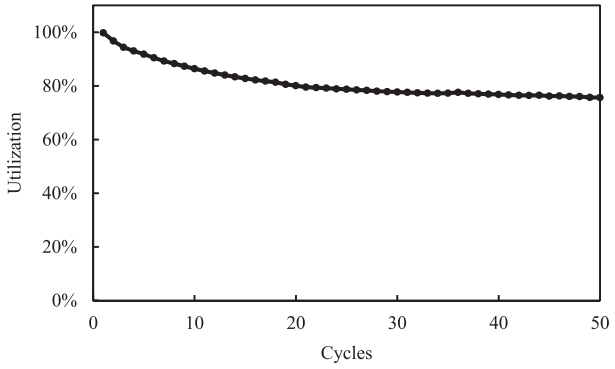

Fig. 5. Discharging capacity decay by 100% DOD cycles for a cell with $Li_{2.6}Cu_{2.1}PO_{6.3}$ cathode active material. The vertical axis was normalized by first discharging capacity (120 mAh g^{-1}).

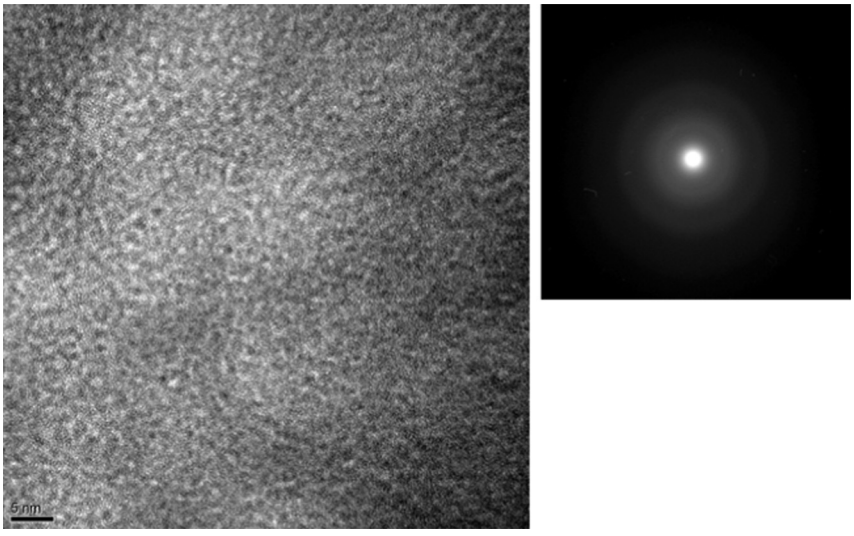

Fig. 3. High resolution TEM and electron beam diffraction image of LiCuPO film. The LiCuPO film was confirmed as amorphous state.

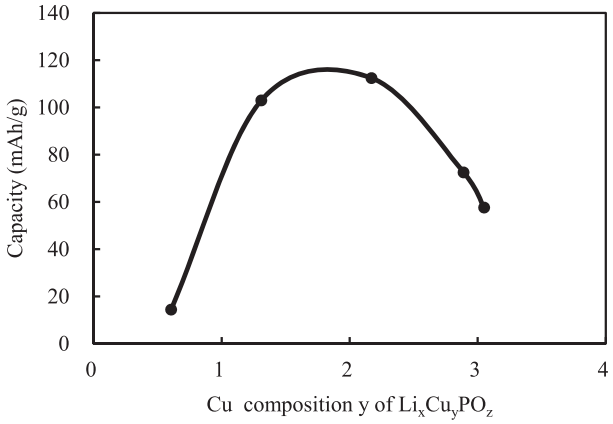

Fig. 6. Composition dependence of LiCuPO capacity.

3.2. a-LiNiPO

Analogous to a-LiCuPO, amorphous LiNiPO was obtained by using Li_3PO_4 and Ni metal target (Li_3PO_4 + Ni), or by using $LiNiO_2$ sintered target instead of Ni metal (Li_3PO_4 + $LiNiO_2$). All films measured by TEM were observed as amorphous similar to LiCuPO films. After optimizing the sputtering power to obtain highest capacity, compositions for films prepared by different target materials were measured as shown in Table 1. Although amorphous materials show no ordering by nature, PO_4, NiO or NiO_2 combinations are considered as dominant nearest neighbors, thus the material is the disordered mixture of above anions. Such experimental analysis will be discussed elsewhere. Comparing the compositions between these LiNiPO in Table 1, LiNiPO (Li_3PO_4 + $LiNiO_2$) showed lower PO_4 ratio against Ni oxide anions. Sputtering using $LiNiO_2$ target enhances the Li and O injecting composition compared with sputtering by Ni metal, which lead to a different optimum composition. However, working mechanism as cathode active material is yet to be clarified.

The Li content inside these materials both correspond to 320 mAh g^{-1} assuming all Li were active. The charge and discharge curves are shown in Fig. 8 for cells with 220 nm thick LiNiPO. Corresponding charging and discharging speed were 1 C for LiNiPO (Li_3PO_4 + $LiNiO_2$) and 2 C for LiNiPO (Li_3PO_4 + Ni), and the obtained capacity were 330 mAh g^{-1} and 170 mAh g^{-1} respectively. The

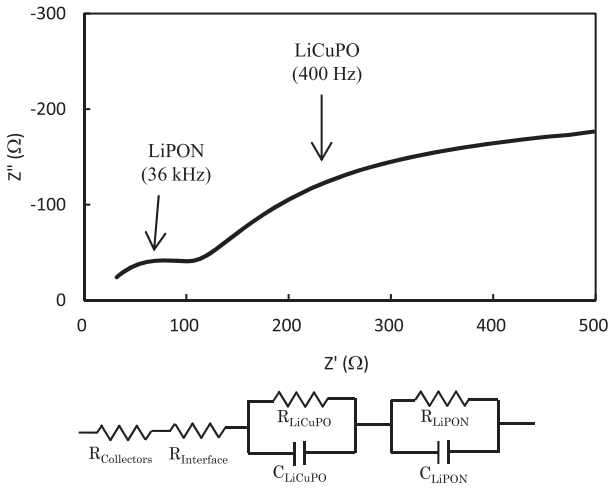

Fig. 7. Impedance spectroscopy of a cell with LiCuPO cathode active material.

Table 1
Compositions of LiNiPO prepared by different sputtering targets measured by combination of ICP-AES and RBS method.

Sputter target	Li content	Ni content	P content	O content
Li_3PO_4 + Ni	2.6	1.3	1	5.9
Li_3PO_4 + $LiNiO_2$	4.2	2.6	1	8.6

capacity of LiNiPO (Li_3PO_4 + $LiNiO_2$) slightly exceeded the theoretical value presumably due to the measurement error of composition or other physical parameters. On the other hand, almost half of Li were encapsulated after charging in LiNiPO (Li_3PO_4 + Ni).

The thickness dependence of the cathode active material capacity for LiNiPO (Li_3PO_4 + $LiNiO_2$) is shown in Fig. 9, all measured at 1 C charging and discharging speed. Discharging capacities were identical to corresponding charging capacities. This result implies that the limitation of cathode active material capacity was induced by the Li content gradation inside the film along depth direction during charging process. Appearance of Li deficient area with high impedance, which appeared at earlier stage for thicker samples, has led to earlier increase in total impedance and resulted as low capacity. This model is consistent with charging speed dependence as shown in Fig. 10 for a 220 nm thick LiNiPO cell. The Li content gradation inside the film may become steeper at higher charging rate, which lead to lower capacity. Although the optimization of thickness and speed are required, a novel amorphous LiNiPO

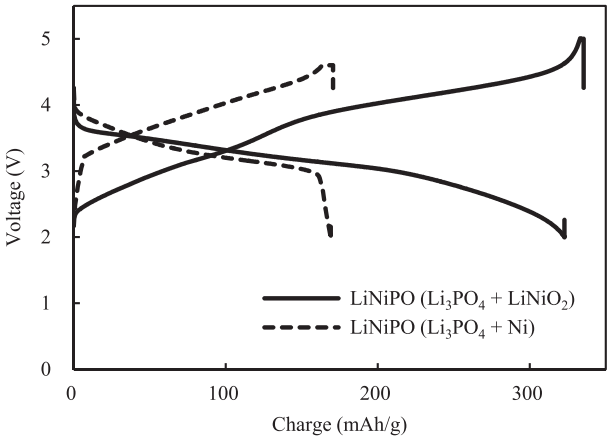

Fig. 8. Charge and discharge curves of LiNiPO cathode active material prepared by different sputtering targets.

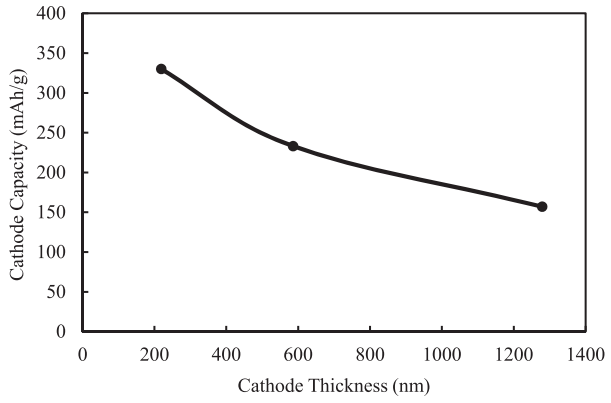

Fig. 9. Thickness dependence of LiNiPO cathode active material capacity.

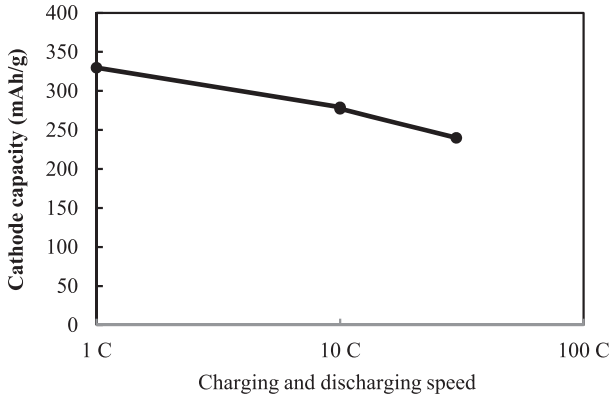

Fig. 10. Charging speed dependence of 220 nm thick LiNiPO cathode active material capacity.

material could be an attractive cathode active material candidate, by showing relatively high capacity of 240 mAh g^{-1} at 220 nm thickness at very fast charging rate of 30 C.

Impedance spectrum was observed for a cell with 1 μm thick LiNiPO to reveal the Li deficient area. Fig. 11(a) shows the spectrum after charging at different speed, 3 C and 30 C, measured at charged state by holding at 5 V (DC). The smaller impedance at higher frequency, as seen in Fig. 11(b) with enlarged scale, are LiPON origin and they were almost stable against charging speed (impedance 72 Ω, center frequency 40 kHz for both charging speed). The lower frequency impedance as seen in Fig. 11(a) are thus originated from LiNiPO, and a clear difference in impedance values were observed. The impedance and center frequency were 7 kΩ and 1 Hz, 440 Ω and 12 Hz, respectively for 3 C and 30 C. The reason for lower impedance at 30 C can be explained from Li deficient area model that the steeper Li content gradation during charging caused Li deficient area with thinner area than that appeared at 3 C charging.

Another observation of the high impedance Li deficient area was performed from discharging process (Fig. 12). After full charging at 3 C and partially discharging at 3 C, the spectra were measured at different state of charge (SOC). At 85% SOC the impedance drastically decreased down to 2.5 kΩ with center frequency of 5 Hz, and at 74% SOC the impedance reached the stable state of 400 Ω with

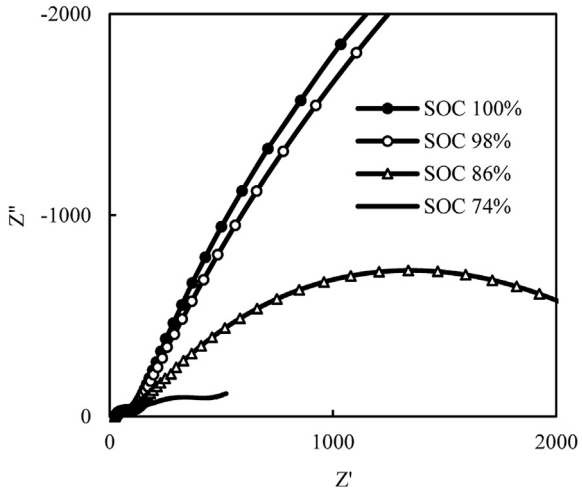

Fig. 12. Impedance spectroscopy measured at different state of charge (SOC). Each curves were taken after full charging (SOC 100%) at 3 C then followed with 3 C discharging speed down to target SOC. There were no drastic changes observed beneath 74%.

25 Hz center frequency and there were no further drastic change in impedance at lower SOC. This result can be construed as Li deficient area being deceased at early stage of discharging process.

Similar to amorphous LiCuPO, LiNiPO showed a wide composition margin as shown in Fig. 13. The optimum Ni content against P was between 1 and 2.5 measured by ICP-AES. Other trial to measure content by XPS method resulted in relatively larger Ni content against P [19], the optimum value was between 3 and 9. Since the surface must be sputter etch cleaned to remove the oxidant or hydrates before the XPS measurement, lighter material such as P may have selectively removed from the surface during the preparation process.

Charging cycle durability is shown in Fig. 14 for a cell with 1 μm thick LiNiPO (Li_3PO_4 + Ni) at 2 C charging and discharging rate. There was no degradation of capacity observed up to about 100 cycles. Further cycling has led to partial delamination of anode collector so the cell structure optimization may lead to improvement.

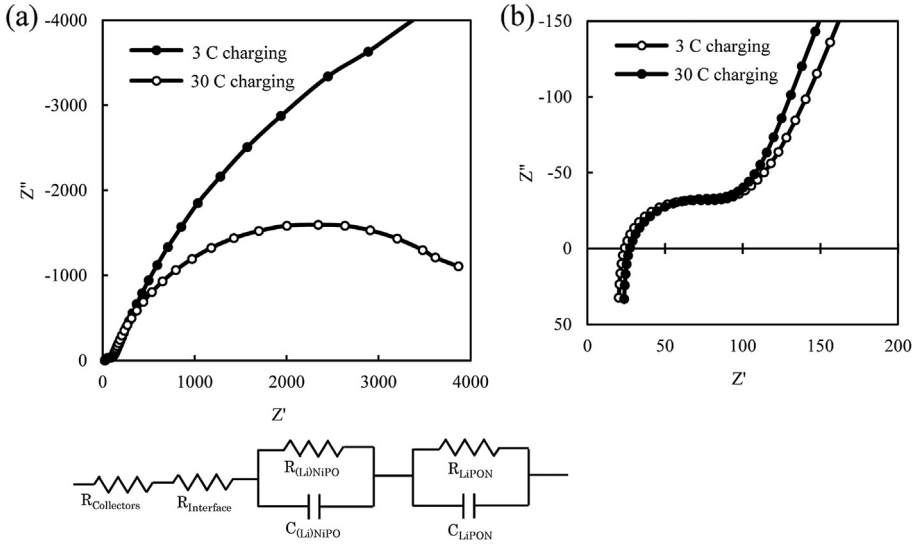

Fig. 11. (a) Full scale and (b) enlarged scale of impedance spectroscopy result of a cell with 1 μm thick LiNiPO cathode active material observed after full charging at 3 C and 30 C speed.

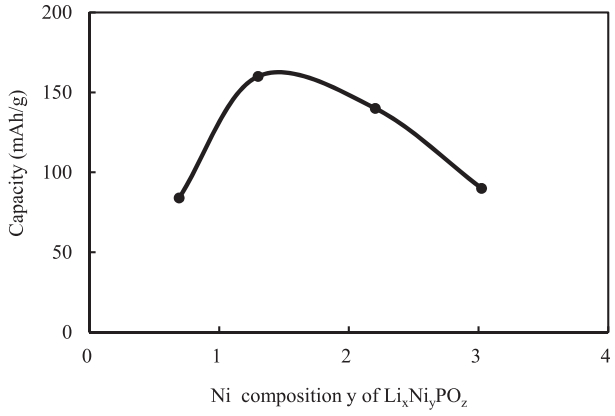

Fig. 13. Composition dependence of LiNiPO capacity measured by ICP-AES.

3.3. Other working metal materials for a-LiMPO

Although the working mechanism is yet unclear, amorphous material composed of Li_3PO_4 together with other metal or metal oxide materials may induce electronic conductivity and turn to work as cathode active material.

Using the similar sputtering method, other metal materials were tested with sputter targets of MgO, Al, Si, Ti, V, Cr, Mn, Fe_2O_3, $LiCoO_2$, ZnO, Ga_2O_3, Zr, Pd, Ag, In_2O_3, SnO_2, Sb, HfO_2, W, and Au. The target material chosen are basically metal if stable, and if the material is not stable or ferromagnetic it may not be suitable for sputtering thus oxides are chosen. DC power is applied for metal targets and RF power for oxides.

Since the metal composition tolerance for LiCuPO and LiNiPO were relatively wide, above metal material were checked in the similar range of M/P composition *y* between 1 and 3. The working metal so far affirmed are M = Mn, Co, Ni, Cu, Pd, Ag, and Au. Other materials are either insulator or the capacity was unpractically small.

Some of the charging and discharging curves were previously reported [19]. The output voltage of these materials were commonly near 3 V.

4. Conclusions

Amorphous $Li_xM_yPO_z$ (LiMPO) were prepared by sputtering Li_3PO_4 together with other metal or metal oxide targets. High energy deposition process has enabled to exploit the unrevealed composition with complete amorphous structure ever reported. The most promising result was obtained with M = Ni. With a wide composition margin the material showed capability to work at 30 C charge and discharging. With optimization of composition the capacity reached above 300 mAh g^{-1}. Preliminary experiment showed that the material is one of the promising materials as fast and high capacity cathode active material.

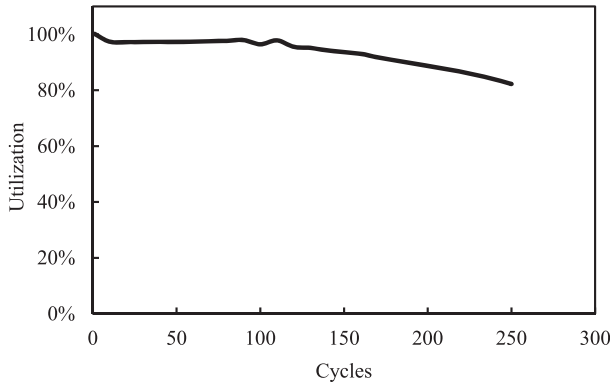

Fig. 14. Cycle durability at 2 C charging and discharging speed. There was almost no decrease in capacity up to 100 cycles.

References

[1] K. Mizushima, P.C. Jones, P.J. Wiesman, J.B. Goodenough, Mater. Res. Bull. 15 (1980) 783–789.
[2] T. Ohzuku, M. Kitagawa, T. Hirai, J. Electrochem. Soc. 137 (1990) 769–775.
[3] A. Yamada, S.C. Chung, K. Hinokuma, J. Electrochem. Soc. 148 (2001) A224–A229.
[4] A.K. Pahdi, K.S. Najundaswamy, J.B. Goodenough, J. Electrochem. Soc. 144 (1997) 1188–1194.
[5] S.K. Martha, H. Sclar, Z.S. Framowitz, D. Kovacheva, N. Saliyski, Y. Gofer, P. Sharon, E. Golik, B. Markovsky, D. Aurbach, J. Power Sources 189 (2009) 248–255.
[6] H. Shigemura, H. Sakaebe, H. Kageyama, H. Kobayashi, A.R. West, R. Kanno, S. Morimoto, S. Nasu, M. Tabuchi, J. Electrochem. Soc. 148 (2001) A730–A736.
[7] E. Peled, Y. Sternberg, A. Gorenshtein, Y. Lavi, J. Electrochem. Soc. 136 (1989) 1621–1625.
[8] J.B. Bates, N.J. Dudney, D.C. Lubben, G.R. Gruzalski, B.S. Kwak, Yu Xiaohua, R.A. Zuhr, J. Power Sources 54 (1995) 58–62.
[9] K. Salloux, F. Chaput, H.P. Wong, B. Dunn, M.W. Breiter, J. Electrochem. Soc. 142 (1995) L191–L195.
[10] J.B. Bates, F.X. Hart, D. Lubben, B.S. Kwak, A. van Zomeren, in: S. Megahed, M. Barnett, L. Xie (Eds.), Rechargeable Lithium and Lithium-ion Batteries, The Electrochemical Soc., Inc., New Jersey, 1995, pp. 342–347.
[11] J.B. Bates, N.J. Dudney, B. Neudecker, A. Ueda, C.D. Evans, Solid State Ionics 135 (2000) 33–45.
[12] B.J. Neudecker, N.J. Dudney, J.B. Bates, J. Electrochem. Soc. 147 (2000) 517–523.
[13] Y. Sabi, K. Takahara, T. Furuya, H. Morioka, M. Adachi, K. Hinokuma, in: The 217th ECS Meeting Abstracts, Vancouver, Canada, 2010. #287.
[14] Y. Sabi, T. Furuya, H. Morioka, Y. Senda, R. Ito, T. Senoo, S. Hayashi, S. Sato, in: The 15th International Meeting on Lithium Batteries Abstracts, Montreal, Canada, 2010. #259.
[15] R. Ito, Y. Sabi, Y. Senda, US Patent Publication US2012/0058385 A1.
[16] S. Hayashi, H. Ono, T. Matsuo, S. Sato, Y. Sabi, S. Onodera, in: The 15th International Meeting on Lithium Batteries Abstracts, Montreal, Canada, 2010. #687.
[17] Y. Sabi, S. Hayashi, H. Morioka, M. Adachi, S. Kusanagi, A. Maesaka, in: The 220th ECS Meeting Abstracts, Boston, USA, 2011. #199.
[18] Y. Sabi, T. Furuya, US Patent Publication US2011/0117433 A1.
[19] Y. Sabi, S. Sato, S. Tsuda, International Patent Publication WO2012/074138.
[20] X. Yu, J.B. Bates, G.E. Jellison Jr., F.X. Hart, J. Electrochem. Soc. 144 (1997) 524–532.

Web references[1]

[21] http://www.sciencedirect.com/science/article/pii/0025540880900124, http://dx.doi.org/10.1016/0025-5408(80)90012-4.
[22] http://jes.ecsdl.org/content/137/3/769.abstract, http://dx.doi.org/10.1149/1.2086552.
[23] http://jes.ecsdl.org/content/148/3/A224.abstract, http://dx.doi.org/10.1149/1.1348257.
[24] http://jes.ecsdl.org/content/144/4/1188.full.pdf+html, http://dx.doi.org/10.1149/1.1837571.
[25] http://www.sciencedirect.com/science/article/pii/S0378775308018442, http://dx.doi.org/10.1016/j.jpowsour.2008.09.090.
[26] http://jes.ecsdl.org/content/148/7/A730.abstract, http://dx.doi.org/10.1149/1.1377593.
[27] http://jes.ecsdl.org/content/136/6/1621.abstract, http://dx.doi.org/10.1149/1.2096981.
[28] http://www.sciencedirect.com/science/article/pii/037877539402040A, SSDI: 0378–7753(94)02040-A.
[29] http://jes.ecsdl.org/content/142/10/L191.abstract, http://dx.doi.org/10.1149/1.2050041.
[30] http://books.google.co.jp/books?id=FPfirvm4jd4C&pg=PA342&lpg=PA342&dq=amorphous+v2o5+cathode+battery&source=bl&ots=PRkOYjA_5v&sig=UMAoszMIVccEeT8TOg6454wmIaU&hl=ja&sa=X&ei=pVYsUdSoMMr3mAWnk4GYDw&ved=0CGIQ6AEwBA#v=onepage&q&f=false, ISBN: 1-56677-087-4.

[1] (All accessed on December 2nd, 2013).

[31] http://www.sciencedirect.com/science/article/pii/S0167273800003271, PII: S0167-2738(00) 00327−1.
[32] http://jes.ecsdl.org/content/147/2/517.abstract, http://dx.doi.org/10.1149/1.1393226.
[33] http://ma.ecsdl.org/content/MA2010-01/4/287.full.pdf+html.
[34] http://ma.ecsdl.org/content/MA2010-03/1/259.full.pdf+html.
[35] http://appft1.uspto.gov/netacgi/nph-Parser?Sect1=PTO1&Sect2=HITOFF&d=PG01&p=1&u=/netahtml/PTO/srchnum.html&r=1&f=G&l=50&s1=20120058385.PGNR.
[36] http://ma.ecsdl.org/content/MA2010-03/1/687.full.pdf+html.
[37] http://ma.ecsdl.org/content/MA2011-02/4/199.full.pdf+html.
[38] http://appft1.uspto.gov/netacgi/nph-Parser?Sect1=PTO1&Sect2=HITOFF&d=PG01&p=1&u=/netahtml/PTO/srchnum.html&r=1&f=G&l=50&s1=20110117433.PGNR.
[39] http://patentscope.wipo.int/search/en/WO2012074138.
[40] http://jes.ecsdl.org/content/144/2/524.abstract, http://dx.doi.org/10.1149/1.1837443.